The Spectral, Structral and Thermal Characterizations of Dimethyl Sulphoxide, Pyridine, Ethanolamine and N-Methyl Formamide Intercalated Kaolinites

Bulent Caglar[a], Beytullah Afsin[b], Erdal Eren[c], Ahmet Tabak[d], Cagri Cirak[e], and Osman Cubuk[a]

[a] Department of Chemistry, Faculty of Arts and Sciences, Erzincan University, 24100 Erzincan, Turkey
[b] Department of Chemistry, Faculty of Arts and Sciences, Ondokuz Mayis University, 55139 Samsun, Turkey
[c] Department of Chemistry, Faculty of Arts and Sciences, Bilecik University, 11200 Bilecik, Turkey
[d] Department of Chemistry, Faculty of Arts and Sciences, Rize University, 53100 Rize, Turkey
[e] Department of Physic, Faculty of Arts and Sciences, Erzincan University, 24100 Erzincan, Turkey

Reprint requests to B. C.; Fax: +904462243016; E-mail: bcaglar55@gmail.com

Z. Naturforsch. **65a,** 1009 – 1019 (2010); received January 26, 2010

The intercalation of dimethyl sulphoxide (DMSO), pyridine (Py), ethanolamine (Ea), and N-methyl formamide (NMF) molecules into the kaolinite interlayers led to an appreciable decrease of 3697 cm^{-1} of the hydroxyl band. The appearance of the peaks at 3662, 3541, and 3504 cm^{-1} proved that the DMSO species are intercalated between the kaolinite layers through forming H-bonds with internal-surface hydroxyl groups. The intensities of the 942 and 796 cm^{-1} bending peaks arising from inner-surface hydroxyls decreased and new vibrational features appeared due to the intercalation of the guest species. The d_{001} value of pure kaolinite was found at 7.18 Å, and the d_{001} values were seen at 11.26, 11.62, 10.77, and 10.67 Å for kaolinite-dimethyl sulphoxide (K-DMSO), kaolinite-pyridine (K-Py), kaolinite-ethanolamine (K-EA), and kaolinite-N-methyl formamide (K-NMF) composites, respectively. The endothermic differential thermal analysis (DTA) peaks at a temperature of 108 – 334 °C reflected the changes in the physicochemical properties of the intercalated species. The thermal stability increase followed the order of K-Py < K-NMF < K-Ea < K-DMSO. Based on the thermal analysis data, the intercalation ratios of the composites above were determined as 80.0, 40.0, 81.6, and 82.0 %, respectively. The specific surface areas are affected by the intercalation geometry of the composites within the gallery spacing. The surface areas of the K-DMSO, K-Py, and K-EA complexes increased whereas the surface area of K-NMF decreased with respect to that of untreated kaolinite.

Key words: Kaolinite; Intercalation; XRD; Thermal Analysis; Inner-Surface Hydroxyls.

1. Introduction

Various processes such as acid activation, organoclay synthesis, intercalation, calcination, and pillaring have been employed to obtain clay products of high quality and desired properties [1 – 5]. An expansion of these processes is the development of new application areas, and the intercalation process is an important step to synthesize the clay-based solid materials. The preparation method of the intercalation complexes may vary depending on the structure, surface area, and swelling capability of clay and the size, polarity, and binding ability of the guest molecules. The guest species are intercalated into kaolinite layers by overcoming the interactions between the kaolinite layers and build H-bonds with inner-surface hydroxyls and inner-surface oxygens. Intercalation complexes have been widely used in paints, catalysis, membranes, liquid crystals, automotive industry, electrical materials, and particular biomedical fields as ion exchangers, selective adsorbents, catalyst, and reinforcing fillers [6 – 9].

Organic and inorganic molecules such as formamide [10 – 14], N-methyl formamide (NMF) [15,16], potassium acetate [17], acetamides [18, 19], hydrazine [11, 17, 20, 21], urea [22], dimethyl sulphoxide (DMSO) [23 – 26], and short chain oil acids [27] may form 'intercalation units' within the unique structure of kaolinite by overcoming the cohesive forces between the free surface hydroxyl groups whereas non-reacting molecules of large size (benzamide [28,29], cylic imides [30], lactam [31], alkoxysilanes [32], pyridine [33], pyridine-carboxylic acids [34], alkyl-

0932–0784 / 10 / 1100–1009 $ 06.00

amines [35]) are entrained by the templates such as DMSO, methanol, and NMF. In addition, the nanocomposite materials prepared by the intercalation of polymer via displacement technique exhibit thermo stability, electric performance, and tensile and barrier properties [36–39]. Therefore, considerable attention has been paid to characterize the precursors to ordered organo-clay composites formed on kaolinite-type minerals [40–45].

In the present study, the structural features of the DMSO, pyridine, ethanolamine, and NMF species intercalated by kaolinite were focussed by using X-ray diffraction (XRD), Fourier transform infrared (FTIR), thermogravimetry-derivative thermogravimetry (TG-DTG), and differential thermal (DT) analyses and surface area measurement techniques.

2. Materials and Methods

Kaolinite (K, Sigma, 212 μm), dimethyl sulphoxide (Fluka, 99.99 %), pyridine (Fluka, 98.00 %), ethanolamine (Fluka, 99.00 %), and N-methyl formamide (Fluka, 99.00 %) were used for preparing the intercalation species.

3 g K was mechanically stirred with 40 ml DMSO at 25 °C for two days in a 50 ml flat-bottomed glass flask and the supernatant was separated by centrifugation at 2000 rpm. The solid product (K-DMSO) was washed with ethanol two times and dried at 60 °C for two days to eliminate the excess of DMSO [23, 40]. The displacement technique (from K-DMSO composite) was used to prepare the Kaolinite-Pyridine (K-Py) intercalate. 1 g K-DMSO was thoroughly mixed with 40 ml pyridine at 60 °C for one day under nitrogen atmosphere. The supernatant was discarded and the precipitate was washed with ethanol. The solid product was dried at 60 °C for two days and sieved to 212 μm [33].

1 g K was thoroughly mixed with 40 ml ethanolamine at 60 °C for one day under nitrogen atmosphere. The supernatant was discarded and the precipitate was washed with ethanol. The solid product (K-EA) was dried at 60 °C for two days at and sieved to 212 μm.

1 g K was thoroughly mixed with 40 ml NMF at 60 °C for one day under nitrogen atmosphere. The supernatant was discarded and the precipitate was washed with ethanol. The solid product (K-NMF) was dried at 60 °C for two days and sieved to 212 μm [16].

FTIR spectra of the bentonite samples were recorded in the spectral region of 4000–200 cm^{-1} on a Mattson-1000 FTIR spectrometer at a resolution of 4 cm^{-1}. XRD patterns were taken on a Rigaku 2000 automated powder diffractometer using Ni-filtered CuKα radiation ($\lambda = 1.54050$ Å; 40 kV and 40 mA). Bragg's law, defined as $n\lambda = 2d\sin\theta$, was used to calculate the crystallographic spacing (d) of the bentonite samples. Thermal analysis runs were performed simultaneously on a Rigaku TG 8110 thermal analyzer combined with TAS 100 (range: 25–1000°) under nitrogen flow (80 ml/min) at a heating rate of 10°/min. Calcinated α-alumina was taken as the reference. Surface areas were measured by adsorption of a special gas mixture (30 % N_2 + 70 % He) at 77 K using a Quantachromosorb instrument. The samples were outgassed at 120° for two hours prior to the surface area measurements.

3. Results and Discussion

3.1. XRD Data of Samples

The d_{001}, d_{020}, $d_{1\bar{1}0}$, $d_{11\bar{1}}$, $d_{1\bar{1}\bar{1}}$, and d_{002} diffractions of the raw kaolinite are seen at 12.32, 19.84, 20.32, 21.08, 21.44, and 24.84° (2θ) with the distances of 7.18, 4.47, 4.37, 4.21, 4.14, and 3.58 Å, respectively (Fig. 1a). When the kaolinite interact with the guest species, an expansion is observed along the c-axis only [17, 39]. New peaks appearing at a distance of 11.27 and 3.76 Å under 7.84 and 23.80° (2θ) (Fig. 1b) signify that the DMSO molecules are directly intercalated into the kaolinite mineral in agreement with the data reported in the literature [23–26]. The basal spacing of kaolinite expands from 7.18 to 11.27 Å (an increase by 4.09 Å), and it may be proposed based on this expansion that one of the methyl groups of DMSO is keying into ditrigonal holes of the siloxane layer [23, 26, 43, 44]. Direct intercalation of pyridine molecules into interlamellar spacing of kaolinite was not successful but they were inserted into the kaolinite interlayer by replacement of the pre-intercalated DMSO species. The d_{001} peak of the resultant K-Py composite was observed at 7.60° (2θ) with a distance of 11.62 Å (Fig. 1c). Keying of pyridine species into the inner layers of kaolinite resulted in an increase of the d_{001} value by $\sim$ 4.44 Å along the c-axis which is below the expected basal spacing value of kaolinite. Since the molecular size of pyridine (6–7 Å) is bigger than this value, the pyridine species has to be tilted slightly with respect to the interlayer plane [33]. The d_{001} value of the K-EA complex

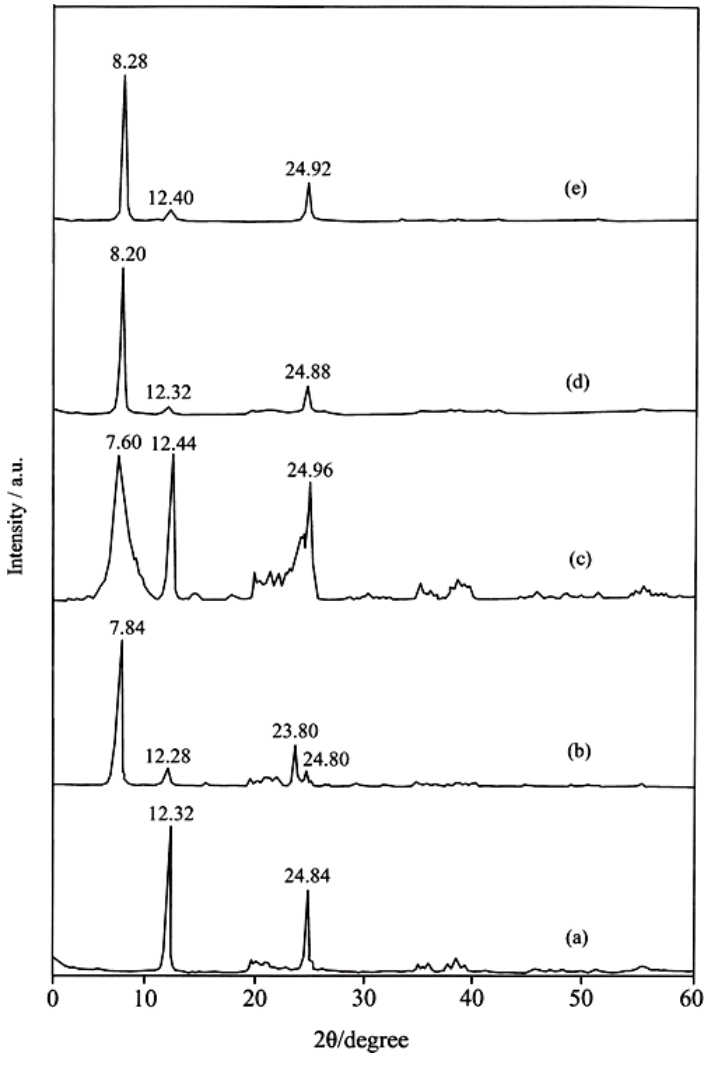

Fig. 1. XRD patterns of (a) Kaolinite, (b) Kaolinite-DMSO, (c) Kaolinite-Py, (d) Kaolinite-Ea, and (e) Kaolinite-NMF.

was determined as 10.77 Å at 8.20° (2θ) which denotes the penetration of the ethanolamine species into the interlayer space of kaolinite (Fig. 1d). On direct insertion of NMF into the interlamellar spacing of kaolinite, a very strong peak with the distance of 10.67 Å corresponding to the newly formed diffraction plane is observed at 8.28° (2θ). Furthermore, the diffraction peaks belonging to the d_{001} and d_{002} planes of kaolinite are observed at 12.40° (2θ) and 24.92° (2θ) with the distances of 7.13 and 3.57 Å, respectively (Fig. 1e). The intensities of these peaks, which were observed for all intercalated complexes here, decreased with the increase of the intercalation ratio. The observation of new diffractions and the expansion of the interlayer spacing of kaolinite by 4.09, 4.44, 3.59, and 3.49 Å (Δd) along the z(c)-axis, respectively, following the insertion of the DMSO, Py, EA, and NMF species may be taken as a clear evidence to the proceeding of a successful intercalation processes. The intercalation ratios calculated from the XRD data of these species are 89,

Table 1. d_{001} distances of intercalation complexes, interlayer expansion (Δd), and intercalation ratio (IR_a) values determined from XRD data and thermal analysis data.

Sample	d_{001} (Å)	Δd (Å)	IR_a based on XRD data (%)	IR_a based on thermal analysis data (%)
K	7.18	–	–	–
K-DMSO	11.27	4.09	89.0	80.0
K-Py	11.62	4.44	50.0	40.0
K-Ea	10.77	3.59	92.6	81.6
K-NMF	10.67	3.49	93.0	82.0

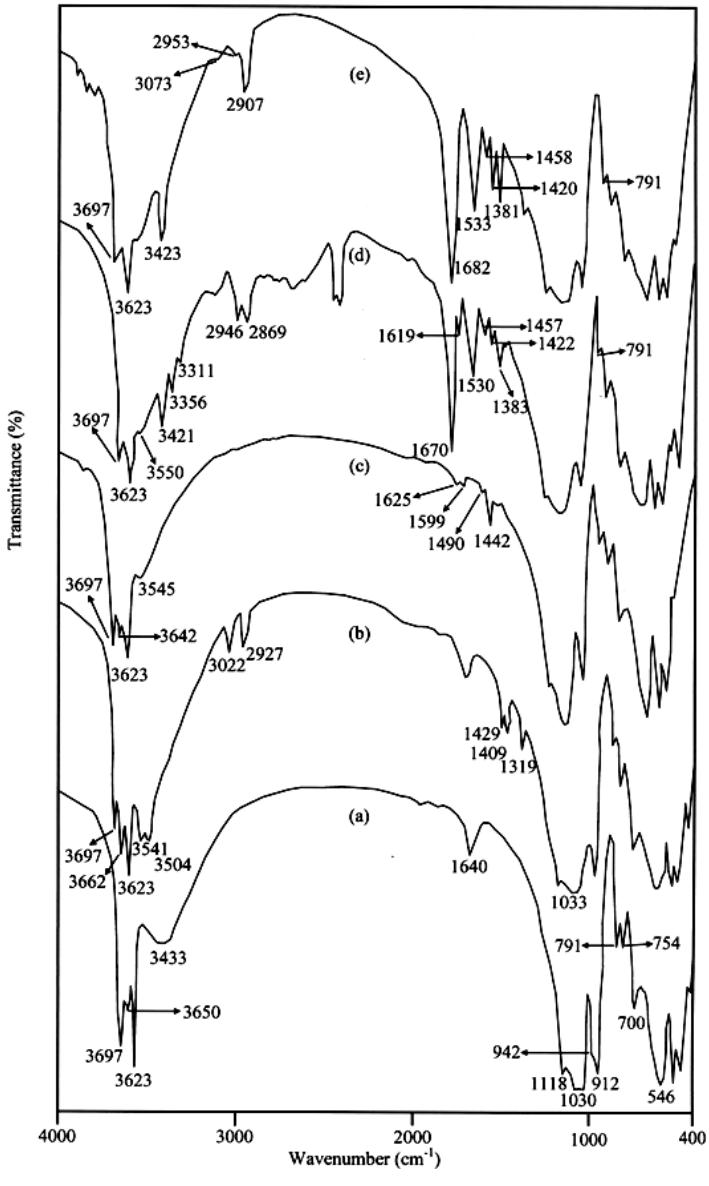

Fig. 2. FTIR spectra of (a) Kaolinite, (b) Kaolinite-DMSO, (c) Kaolinite-Py, (d) Kaolinite-Ea, and (e) Kaolinite-NMF.

50, 92, and 92 %, respectively [28]. The amount of the NMF species intercalated by kaolinite is higher than the other molecules (Table 1).

3.2. FTIR Spectra of Samples

The kaolinite mineral has four IR-active bands centered at 3697, 3671, 3650, and 3623 cm^{-1}, originating from different hydroxyl groups (Fig. 2a) [46–48]. In the raman spectrum of the kaolinite mineral, an additional raman active but not IR-active band exists at 3684 cm^{-1} [49, 50]. The three higher frequency vibrational peaks belong to the stretches of the inner-surface hydroxyl groups whereas the peak at a lower frequency (3623 cm^{-1}) corresponds to the inner-sheet hydroxyl groups. The 3697 and 3671 cm^{-1} bands are attributed to coupled antisymmetric and symmetric vibrations [46–49]. The peak at 3650 cm^{-1} originates from the combination of the OH_2 and OH_4 groups or adsorbed water species [51]. The peak at 3684 cm^{-1} depends on the orientations and positions of both the inner-sheet and inner-surface hydroxyl groups. This

peak has also been observed due to the orientation of the H-bonds between the inner-surface hydroxyls and the siloxane layer in vicinity [12]. However, the peak at 3650 cm^{-1} may be assigned to the out-of-phase analogue of the in-phase vibration located at 3684 cm^{-1} [50].

The insertion of DMSO into the interlayer spacing of kaolinite resulted in a significant decrease of the intensity of the inner-surface hydroxyl band at 3697 cm^{-1}, and three new sharp peaks emerge at 3662, 3541, and 3504 cm^{-1} (Fig. 2b). The changes in the intensities and positions of these peaks depend on the interlayer characteristics of the clay minerals [27]. When the intercalation ratio of DMSO is increased, the peak at 3697 cm^{-1} loses intensity whereas the peaks at 3662, 3541, and 3504 cm^{-1} become stronger [23, 52]. The inner-layer hydroxyl stretching peak at 3623 cm^{-1} is not affected by the presence of DMSO species in general [52]. However, the intensity of this peak changes when the kaolinite-DMSO complex is formed [25]. This means that the DMSO species interact with the relatively free inner-surface hydroxyl groups and thus, new hydrogen bonds are built in a three-dimensional structure wherein the DMSO species are triply H-bonded and situated above the vacancies in the octahedral sheet of the kaolinite [23, 25]. The antisymmetric and symmetric C-H stretching peaks at 2994 and 2913 cm^{-1}, the antisymmetric CH_3 deformation peaks at 1438, 1414, and 1404 cm^{-1} and the symmetric deformation CH_3 peak at 1314 cm^{-1} of pure DMSO molecules shift to 3022 and 2937 cm^{-1}; and to 1429, 1409, and 1395 cm^{-1} and 1319 cm^{-1}, respectively, after intercalation of DMSO (Table 2) [53]. The shifts to low energy regions of these C-H stretching and bending vibrations are caused by the repulsion between the carbon atom of the methyl group and the neighbouring dipoles (the OH groups and the surface oxygen atoms of the clay) [25, 43, 44]. In addition, the bending mode of the inner-surface hydroxyl (Al-O-H) groups at 942 cm^{-1} is weakened following the insertion of DMSO. The presence of the ν(S=O) peak at 1033 cm^{-1} and the absence of the symmetric C-S vibration in the spectrum of the K-DMSO composite point out that the H-bonding occurs through the oxygen atom of the DMSO molecule.

The treatment of the K-DMSO composite with pyridine caused the disappearance of the characteristic peaks of DMSO, the decrease of the intensity of the hydroxyl peak at 3697 cm^{-1} and gave rise to the emergence of new peaks at 3642 and 3545 cm^{-1} in the OH vibrational region (Fig. 2c). The peak at 3642 cm^{-1} originates from the formation of H-bonding between pyridine and inner-surface hydroxyl groups of kaolinite. The weakening of the stretching and deformation peaks of the inner-surface hydroxyls at 3697 and 942 cm^{-1}, respectively, prove the formation of H-bonding. The H-bonded pyridine species gave rise to the peaks at 1440 and 1590 cm^{-1} whereas the pyridine species coordinated to the Lewis and Bronsted acidic centres result in the peaks at 1450, 1610, 1490 and 1540, 1490, 1635 cm^{-1}, respectively (Fig. 2c and Table 2). These bending peaks are expected to be affected by the interlayer positions of the adsorbed pyridine species. Hence, the intensity variations and shifts to higher frequencies of the Si-O-Si stretching peaks depend on the strength of the interactions between the oxygen plane and the intercalated pyridine species. Thus, the shift of the peak belonging to pure pyridine at 1440 cm^{-1} to 1442 cm^{-1} and the appearance of

Table 2. Peak assignments of vibrational features of K-DMSO, K-Py, K-EA, and K-NMF complexes.

Peak assignment	Experimental [53]	Experimental
	DMSO	K-DMSO
ν_{CH}	2994	3022
ν_{CH}	2913	2937
$\delta_{HCH} + \tau_{HCSC}$	1438	1429
$\delta_{HCH} + \tau_{HCSC}$	1414	1409
δ_{HCH}	1314	1319
	Py	K-Py
ν_{CH}	3079	–
ν_{CH}	3029	–
ν_{CH}	3002	–
$\nu_{C} + \nu_{NC} + \delta_{CNC} + \delta_{HCN}$	1580	1599
$\delta_{HCN} + \delta_{HCC} + \nu_{NC} + \nu_{CC}$	1484	1490
$\delta_{HCC} + \delta_{HCN}$	1440	1442
$\delta_{HCN} + \delta_{HCC}$	1384	–
	Ea	K-Ea
ν_{OH}	3642	3550
ν_{NH}	3351	3356
ν_{NH}	3286	3311
ν_{CH}	2935 – 2863	2946 – 2889
δ_{HNH}	1601	1619
δ_{HCH}	1457	1530
$\delta_{HCN} + \delta_{HOC} + \tau_{HCCO}$	1360	1383
	NMF	K-NMF
ν_{NH}	3295	–
ν_{CH}	3067	3073
ν_{CH}	2944	2953
ν_{CH}	2878	2907
$\nu_{O=C}$	1689	1682
$\delta_{HCH} + \tau_{NCNC} + \delta_{HNC}$	1545	1533
δ_{HCO}	1387	1381
$\nu_{NC} + \delta_{HNC} + \delta_{OCN}$	1249	–

ν: stretching; δ: in plane bending; τ: torsion.

Table 3. Thermal analysis data of K, K-DMSO, K-Py, K-EA, and K-NMF complexes.

Sample	Temperature range (°C)	Mass loss (%)	$DTA_{max.}$ (endo)
K	397 – 628	12.9	504
	950 – 990	0.0	987(exo)
K-DMSO	50 – 203	18.24	166
	235 – 606	13.07	512
	950 – 990	0.0	984(exo)
K-Py	50 – 199	9.0	108 – 156
	400 – 540	12.1	507
	950 – 990	0.0	984(exo)
K-Ea	50 – 195	9.36	154
	195 – 400	6.24	334
	400 – 545	9.73	474
	950 – 990	0.0	978(exo)
K-NMF	50 – 203	15.35	144
	366 – 615	17.50	475
	950 – 990	0.0	987(exo)

the peak at 1599 cm^{-1} show the H-bonding between the intercalated pyridine species and inner-surface hydroxyl groups since the pyridinium species do not have any prominent peak in the ring frequency region but the H-bonded pyridine species exhibit a number of peaks in this region [54 – 60].

Following direct intercalation of ethanolamine into kaolinite layers, the intensity of the hydroxyl peak at 3697 cm^{-1} decreased and new peaks at 3550, 3421, 3356, and 3311 cm^{-1} were observed (Fig. 2d). The peaks at 3356 and 3311 cm^{-1} which are attributed to the N-H stretches of K-EA species are observed at 3351 and 3286 cm^{-1} for liquid ethanolamine and shifted to higher frequencies during the intercalation process. However, there seemed no intensity changes of these peaks and it is understood that the ethanolamine molecule is bound to the surface OH groups of kaolinite by H-bonding and the vibrational peak emerged at 3421 cm^{-1} in parallel with this which originates from the intercalated ethanolamine species proves the occurrence of a successful intercalation process. The stretching peak of the interlayer hydroxyl groups at 3623 cm^{-1} was not affected by the process. The C-H stretching peaks which appeared at 2935 and 2863 cm^{-1} for pure liquid ethanolamine shifted to the higher frequencies of 2946 and 2869 cm^{-1}. The N-H stretching, the C-H bending and C-H stretching peaks of liquid ethanolamine at 1601, 1457, and 1360 cm^{-1} shifted to 1619, 1530, and 1383 cm^{-1}, respectively, for K-EA complex, as a result of the intercalation process (Table 3). The NH deformation peak at 1670 cm^{-1} shifted to higher frequency due to the repulsion between the NH group of the intercalation complex and oxygen atoms of the siloxane layers.

The intensity of the OH peak of kaolinite at 3697 cm^{-1} decreased strikingly and a new vibrational feature developed at 3423 cm^{-1} on intercalation of NMF molecule into the interlayer spacing (Fig. 2e). In addition, there occurred no variations in the stretching peak at 3623 cm^{-1} of inner-sheet hydroxyls of kaolinite. The significant intensity loss of the peak of inner-surface hydroxyls at 3697 cm^{-1} and the emergence of a new feature at 3423 cm^{-1} at the expense of the former peak show that the intercalation of the NMF species occurs through H-bonding. The maximium intensity loss of the peak at 3697 cm^{-1} compared to other kaolinite complexes in this study points out that the NMF molecule interacts primarily with the perpendicular inner-surface hydroxyl groups. The C=O stretching peak of liquid NMF at 1689 cm^{-1} shifted to 1682 cm^{-1} for the K-NMF complex, which indicates that the binding occurs through the carbonyl oxygen of the molecule. But, the CN stretching peak of liquid NMF at 1387 cm^{-1} was observed at 1381 cm^{-1} for the K-NMF complex (Table 2). If the NMF molecule was bound to kaolinite via the oxygen atom of carbonyl, the C-N stretching peak would be expected to shift to the higher frequency. This means that the NMF molecule forms an H-bonding with inner-surface hydroxyls via the carbonyl oxygen and it also forms an H-bond with the oxygen of the siloxane layer via the NH group. This type of binding may explain the frequency increase of the C-N stretching peak. In addition, the N-H deformation peak of liquid NMF at 1544 cm^{-1} is seen at a lower frequency at 1533 cm^{-1}; the C-H stretching peaks of liquid NMF at 3067, 2944, and 2878 cm^{-1} shifted to 3073, 2953, and 2907 cm^{-1}, respectively, whereas the C-H deformation peaks at 1460 and 1415 cm^{-1} are located at 1458 and 1415 cm^{-1}, respectively, following the intercalation of the NMF species. Furthermore, the intensity loss of the bending peak of the inner-surface hydroxyl at 942 cm^{-1} verifies that the NMF molecule forms H-bonds with inner-surface hydroxyls of kaolinite.

3.3. Thermal Analysis Data of Samples

An endothermic mass loss by 12.9 % with a DTA peak at 504 °C corresponding to the dehydroxylation stage of kaolinite is observed in the temperature range of 397 – 628 °C (Fig. 3a). The DTA peak centred at 987 °C is not accompanied by any mass losses on the

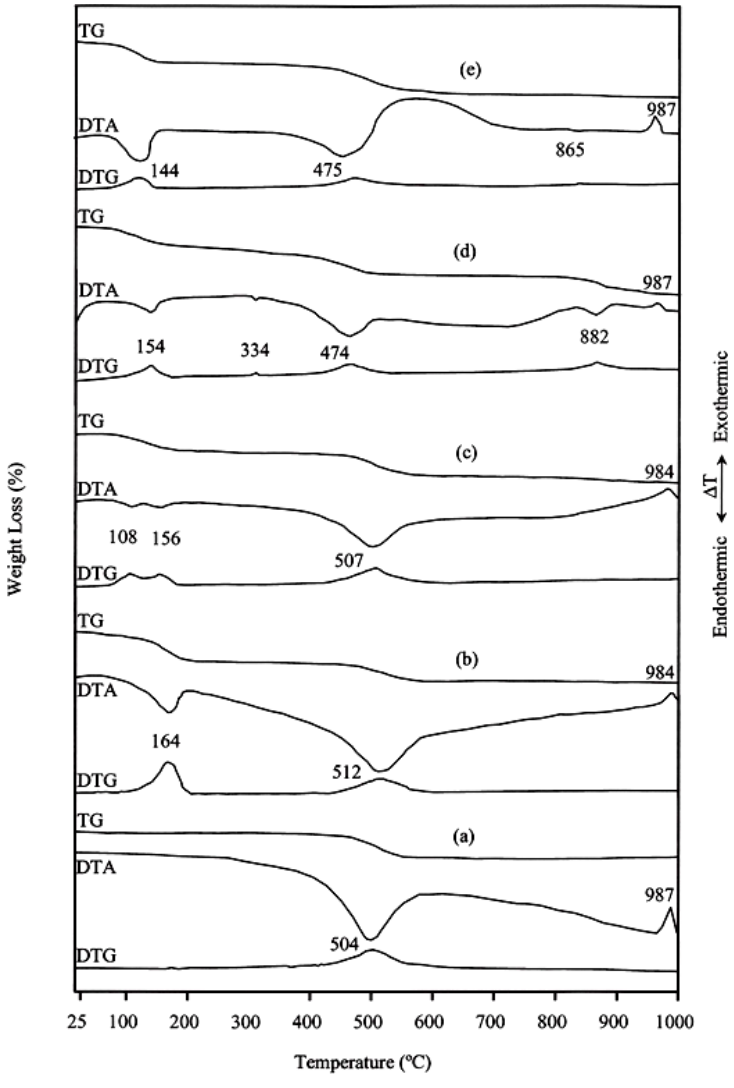

Fig. 3. DTA, DTG, and TG curves of (a) Kaolinite, (b) Kaolinite-DMSO, (c) Kaolinite-Py, (d) Kaolinite-Ea, and (e) Kaolinite-NMF.

TG and DTG curves. A phase transition of dehydroxilated kaolinite to γ-alumina and/or mullite is likely to occur at this temperature [29]. For K-DMSO, a mass loss by 13.1 % in the range of 235 – 606 °C on the DTG curve and an exothermic DTA maximum of 984 °C are observed similar to that of untreated kaolinite (Fig. 3b). These peaks correspond to the dehydroxilation of kaolinite and the formation of γ-alumina and/or mullite similar to that of kaolinite. In addition to those variations, a DTG maximum of 164 °C with a mass loss by 18.2 % in the range of 50 – 203 °C on the TG curve is observed (Table 3). This mass loss emerges as an endothermic feature on the DTA curve and corresponds to the intercalated DMSO species. Based on the intercalation ratio of DMSO which was determined as 80 % using the thermal analysis results (Table 1), the structure of the K-DMSO complex may be represented by the formulae $Al_2Si_2O_5(OH)_4[(CH_3)SO]_{0.8}$.

Following the replacement of the DMSO composites by pyridine species, the DTG peak at 507 °C and the DTA peak at 984 °C are observed on the thermal analysis curves of the newly obtained K-Py complex (Fig. 3c). The peak maxima at 108 and 156 °C with a total mass loss by 9.0 % indicate a two-step decomposition process in the temperature range of 50 – 199 °C (Table 3). The first stage which occurs with a mass loss of 4.2 % in the range of 80 – 126 °C and the second stage that occurs with a mass loss of 4.6 % in the

range of 126 – 199 °C are due to the removal of the intercalated pyridine species and indicate that pyridine molecule interacts with the K-DMSO complex. Referring to the intercalation ratio of 40 % obtained from the thermal analysis data (Table 1), the K-Py complex may be represented by the formulae $Al_2Si_2O_5(OH)_4$-$(C_5H_5N)_{0.4}$.

On the TG curve of the K-EA complex which is obtained by insertion of ethanolamine into the interlayer spacing of kaolinite, the mass losses by 9.5, 6.2, and 9.7 % are observed in the temperature intervals of 50 – 195, 195 – 400, and 400 – 545 °C, respectively (Fig. 3d). These mass losses correspond to the endothermic DTA peaks centred at 154, 334, and 474 °C, respectively (Table 3). The dehyroxilation process occurs in two steps when ethanolamine species are intercalated into the interlayer spacing of kaolinite. The DTA peak maxima of 154 and 334 °C which are accompanied by a total mass loss of 15.6 % are due to the removal of ethanolamine molecules. Referring to the intercalation ratio of 81.6 % based on this mass loss (Table 1), the K-EA complex may be represented by the formulae $Al_2Si_2O_5(OH)_4(OHCH_2CH_2NH_2)_{0.816}$. The DTG peak centred at 474 °C is accompanied by a mass loss of 9.7 % which originates from dehydroxilation of kaolinite. The exothermic DTA peak at 972 °C belongs to the phase transition resulting in γ-alumina and/or mullite structures similar to the intercalation complexes above. In addition to this, a distinct endothermic feature which was centred at 882 °C in the temperature range of 545 – 906 °C with a mass loss by 8.8 % on the TG curve of the K-EA complex may be inferred from dehyroxilation of kaolinite since the dehyroxilation process of kaolinite takes place between 400 and 1000 °C.

K-NMF gives rise to a peak centred at 510 °C in the range of 366 – 615 °C on the TG and DTG curves which is accompanied by a mass loss of 17.5 %. This loss which is represented by an endothermic DTA peak at 475 °C belongs to the dehyroxilation of kaolinite. The exothermic DTA peak at 987 °C shows the formation of γ-alumina and/or mullite from kaolinite (Fig. 3e and Table 3). Furthermore, the endothermic DTA peak centred at 144 °C is associated with a mass loss of 15.4 % in the temperature range of 50 – 203 °C corresponding to the desorption of molecular NMF species. Based upon the intercalation ratio of NMF calculated as 82 % from the thermal analysis data (Table 1), the K-NMF complex may be designated as $Al_2Si_2O_5(OH)_4(CH_3NHCOH)_{0.82}$.

Table 4. Specific surface areas of intercalation complexes.

Sample	Surface area (m^2/g)
K	12.8 ± 0.3
K-DMSO	14.6 ± 0.3
K-Py	15.1 ± 0.3
K-Ea	14.2 ± 0.3
K-NMF	10.8 ± 0.3

3.4. Surface Areas of Samples

The specific surface area of the kaolinite sample used in this study was determined to be 12.08 ± 0.3 m^2/g (Table 4), showing a mesoporous or macroporous structure rather than a microporous structure. It may be seen from Table 4 that the surface areas of the K-DMSO, K-Py, and K-EA complexes increase while that of K-NMF decreases in comparison with the surface area of kaolinite. The possible interca-

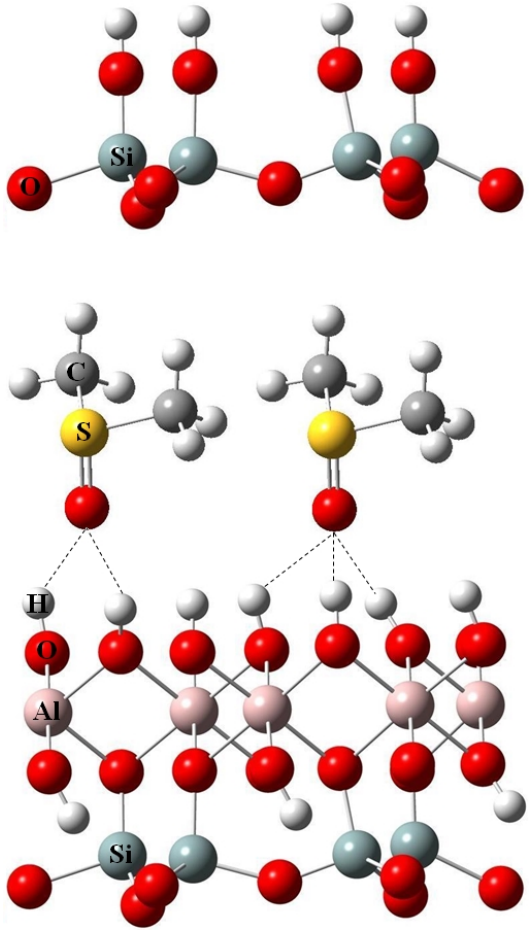

Fig. 4 (colour online). Schematic representation of Kaolinite-DMSO.

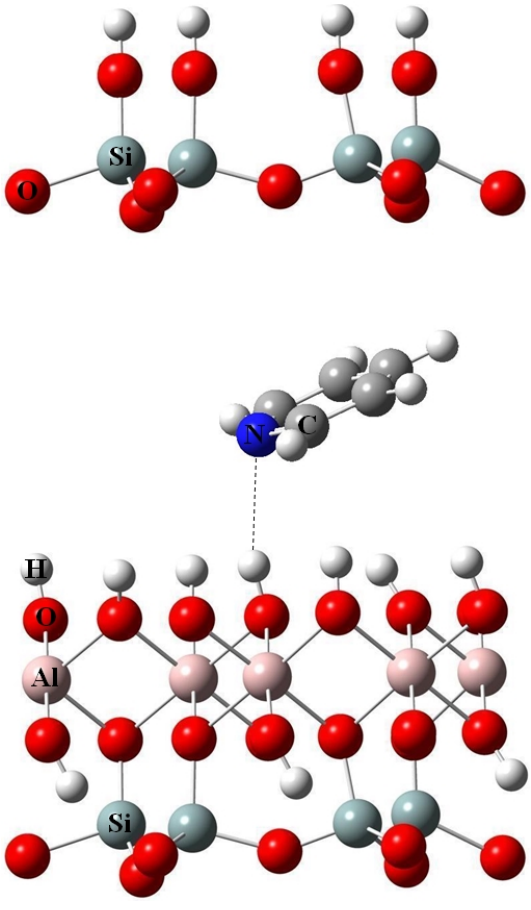

Fig. 5 (colour online). Schematic representation of Kaolinite-Py.

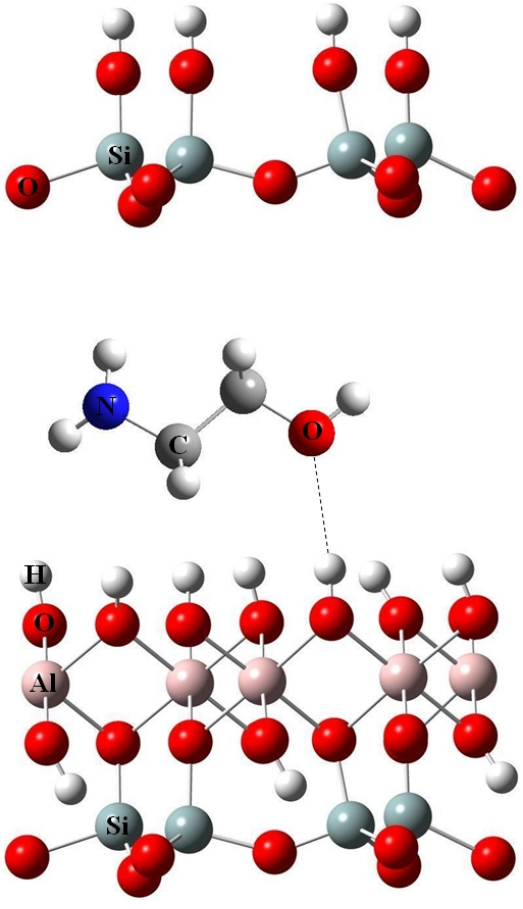

Fig. 6 (colour online). Schematic representation of Kaolinite-Ea.

lation geometries of DMSO, pyridine, ethanolamine, and N-methyl formamide species within the interlayer spacing of kaolinite are illustrated as models in Figures 4 – 7. The organic molecules are located in the interlayer spacing form smaller pores (meso- and micropores) and thus, increase the surface of pure kaolinite depending on the amount of the interlayer expansion and also the intercalation position of the guest species within the interlayer spacing of the clay mineral. The specific surface area of K-Py is bigger than those of K-DMSO and K-EA because of the larger interlayer expansion and the formation of smaller sized interlayer pores on the hydroxyl plane as a result of the H-bonding between inner-surface hydroxyls and pyridine species. The higher specific surface area of K-DMSO compared with that of the K-EA complex may be explained by the induction of a greater expansion by the DMSO species intercalated in different geometries in the interlayer spacing.

The K-NMF complex is expected to have a higher surface area compared with that of kaolinite since its interlayer spacing is larger than that of kaolinite. However, the smaller specific surface area of this complex which is similar to that of the K-Benzamide complex [29] implicates that the interlayer configuration of the intercalated species is more effective than the interlayer distance in determining the surface of the organo-kaolinite complex. It is possible to say that the larger the molecule the bigger the number of micro- and mesopores blocked by the intercalated species. The intercalation geometry of the NMF species within the interlayers of kaolinite is shown as a model in Figure 7. The NMF molecule is bound both to the surface hydroxyls in the hydroxyl plane and the oxygen atoms in the oxygen plane through H-bonding in a bridging

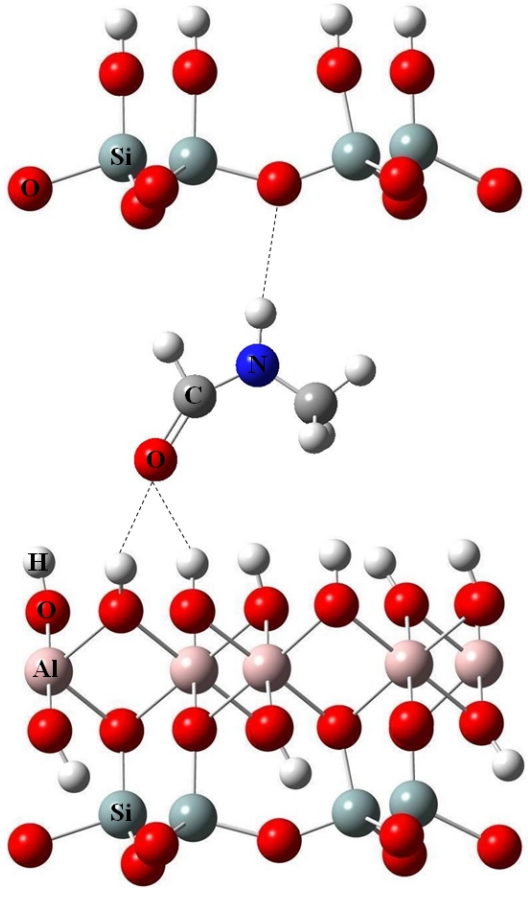

Fig. 7 (colour online). Schematic representation of Kaolinite-NMF.

position that will decrease the strength of nitrogen adsorption.

4. Conclusions

The following general conclusions may be derived from the data of all the samples presented in this study. The specific surface area was affected by the intercalation geometry most during the intercalation process. If the molecule interacted with a monolayer and formed micro- or mesopores, the surface area increased whereas the interaction with a double layer prevented the access of inert gas (nitrogen) to the pores and the surface area decreased. The intensity decrease of the peak at 3697 cm^{-1} and the variations in the intensity ratios of the peaks at 3697 and 3623 cm^{-1} during the intercalation processes are related to the intercalation ratios of the molecules. The intercalation ratios of the molecules determined from the intensity ratio of these peaks followed the order: NMF $\cong$ Ethanolamine $>$ DMSO $>$ Pyridine. The intensity losses of the bending peaks of the inner-surface hydroxyl and the M-OH groups of kaolinite point out the presence of the interaction between the intercalated species and the inner-surface hydroxyl groups of kaolinite. Thermal analysis results support the XRD data proving that the smaller the size of the guest molecule the higher is the intercalation ratio.

Acknowledgement

The Research Foundation of Ondokuz Mayis University is gratefully acknowledged for the financial support to this work under the Project No. F238.

[1] M. Önal and Y. Sarıkaya, Powder Technol. **172**, 14 (2007).
[2] S. M. Koh and J. B. Dixon, Appl. Clay Sci. **18**, 111 (2001).
[3] S. A. Solin, Annu. Rev. Mater. Sci. **27**, 89 (1997).
[4] H. Noyan, M. Önal, and Y. Sarikaya, Clays Clay Miner. **54**, 381 (2006).
[5] M. J. Hernando, C. Pesquera, C. Blanco, I. Benito, and F. Gonzalez, Appl. Catal. **141**, 175 (1996).
[6] H. H. Murray, Appl. Clay Sci. **17**, 207 (2000).
[7] L. P. Meier, R. Nueesch, and F. T. Madsen, J. Colloid Interface Sci. **238**, 24 (2001).
[8] M. Kawasumi, N. Hasegawa, A. Usiki, and A. Okada, Appl. Clay Sci. **15**, 93 (1999).
[9] H. Zhao and G. F. Vance, Water Res. **32**, 3710 (1998).
[10] A. Weiss, W. Thielepape, and H. Orth, Proc. Int. Clay Conf. **1**, 277 (1966).
[11] J. Kristof, R. L. Frost, J. T. Kloprogge, E. Horvath, and M. Gabor, J. Therm. Anal. Cal. **56**, 885 (1999).
[12] R. L. Frost, J. Kristof, E. Horvath, and J. T. Kloprogge, Spectrochim. Acta, A **56**, 1191 (2000).
[13] A. Michalkova, D. Tunega, and L. T. Nagy, J. Mol. Struc. **581**, 37 (2002).
[14] R. L. Frost, E. Horvath, E. Mako, J. Kristof, and T. Cseh, J. Colloid Interface Sci. **265**, 386 (2003).
[15] S. Olejnik, A. M. Posner, and J. P. Quirk, Clays Clay Miner. **19**, 83 (1971).
[16] B. P. Kelleher, D. Sutton, and T. F. O'Dwyer, J. Colloid Interface Sci. **255**, 219 (2002).
[17] R. L. Ledoux and J. L. White, J. Colloid Interface Sci. **21**, 127 (1966).

[18] S. Olejnik, A. M. Posner, and J. P. Quirk, J. Colloid Interface Sci. **37**, 536 (1971).
[19] R. L. Frost, J. Kristof, G. N. Paroz, and J. T. Kloprogge, Phys. Chem. Miner. **26**, 257 (1999).
[20] M. D. Ruiz Cruz and F. Franco, Clays Clay Miner. **48**, 63 (2000).
[21] E. Horvath, J. Kristof, R. L. Frost, A. Redey, V. Vagvölgyi, and T. Cseh, J. Therm. Anal. Cal. **71**, 707 (2003).
[22] E. Mako, J. Kristof, E. Horvath, and V. Vagvölgyi, J. Colloid Interface Sci. **330**, 367 (2009).
[23] J. G. Thompsom and C. Cuff, Clays Clay Miner. **33**, 490 (1985).
[24] S. Olejnik, L. A. G. Alymore, A. M. Posner, and J. P. Quirk, J. Phys. Chem. **72**, 241 (1968).
[25] M. Raupach, P. F. Baron, and J. G. Thompson, Clays Clay Miner. **35**, 208 (1987).
[26] X. Zhang and Z. Xu, Mater. Lett. **61**, 1478 (2007).
[27] B. K. G. Theng, John Wiley and Sons, New York 1974, pp. 243 – 260.
[28] J. E. Gardolinski, L. P. Ramos, G. P. Souza, and F. Wypych, J. Colloid Interface Sci. **221**, 284 (2000).
[29] B. Caglar, B. Afsin, and A. Tabak, J. Therm. Anal. Cal. **87**, 429 (2007).
[30] T. A. Elbokl and C. Detellier, J. Colloid Interface Sci. **323**, 338 (2008).
[31] Y. Sugahara, S. Kitano, S. Satokawa, K. Kuroda, and C. Kato, Bull. Chem. Soc. Jpn. **59**, 2607 (1986).
[32] L. R. Avila, E. H. Faria, K. J. Ciuffi, E. J. Nassar, P. S. Calefi, M. A. Vicente, and R. Trujillano, J. Colloid Interface Sci. **341**, 186 (2010).
[33] Y. Sugahara, S. Satokawa, K. Yoshioka, K. Kuroda, and C. Kato, Clays Clay Miner. **37**, 143 (1989).
[34] E. H. Faria, O. J. Lima, K. J. Ciuffi, E. J. Nassar, M. A. Vicente, R. Trujillano, and P. S. Calefi, J. Colloid Interface Sci. **335**, 210 (2009).
[35] Y. Komori, Y. Sugahara, and K. Kuroda, Appl. Clay. Sci. **15**, 241 (1999).
[36] Y. Sugahara, S. Satokawa, K. Kuroda, and C. Kato, Clays Clay Miner. **38**, 137 (1990).
[37] T. Itagakı, A. Matsumura, M. Kato, A. Usukı, and K. Kuroda, J. Mater. Sci. Lett. **20**, 1483 (2001).
[38] B. Zhang, Y. Li, X. Pan, X. Jia, and X. Wang, J. Phys. Chem. Solids **68**, 135 (2007).
[39] Y. Li, B. Zhang, and X. Pan, Compos. Sci. Technol. **68**, 1954 (2008).
[40] P. M. Costanzo, C. V. Clenency, and R. F. Giese, Clays Clay Miner. **28**, 155 (1980).
[41] J. Kristof, R. L. Frost, A. Felinger, and J. Mink, J. Mol. Struc. **410**, 199 (1997).
[42] R. L. Frost and J. Kristof, Clays Clay Miner. **45**, 551 (1997).
[43] S. Yariv and I. Lapides, J. Therm. Anal. Cal. **94**, 433 (2008).
[44] I. Lapides and S. Yariv, J. Therm. Anal. Cal. **97**, 19 (2009).
[45] J. J. Tunney and C. Detellier, J. Mater. Chem. **6**, 1679 (1996).
[46] V. C. Farmer, Science **145**, 1189 (1964).
[47] V. C. Farmer and J. D. Russell, Spectrochim. Acta. **20**, 1149 (1964).
[48] V. C. Farmer, in The Infrared Spectra of Minerals, (Ed. V. C. Farmer), Mineralogical Society, London 1974, p. 331.
[49] C. I. Fialips, S. Petit, A. Decarreau, and D. Beaufort, Clays Clay Miner. **48**, 173 (2000).
[50] R. L. Frost and S. J. Van Der Gaast, Clay Miner. **32**, 471 (1997).
[51] D. L. Bish and C. T. Johnston, Clays Clay Miner. **41**, 297 (1993).
[52] J. M. Adams, Clays Clay Miner. **31**, 352 (1983).
[53] Agros Organics, Electronic Web Page 2009 (www.agros.com).
[54] S. Akyüz, T. Akyüz, and J. E. D. Davies, J. Mol. Struc. **482**, 49 (1999).
[55] A. Tabak and B. Afsin, Ads. Sci. Technol. **18**, 673 (2001).
[56] A. J. Lopez, E. R. Castellon, M. Trombetta, and G. Busca, J. Mol. Catal. A: Chemical. **168**, 247 (2001).
[57] L. Jankovich and P. Komadel, J. Catal. **218**, 227 (2003).
[58] M. Kurian and S. Sugunan, Micropor. Mesopor. Mater. **83**, 25 (2005).
[59] B. Tyagi, C. D. Chudasama, and R. V. Jasra, Appl. Clay Sci. **31**, 16 (2006).
[60] C. R. Reedy, G. Nagendrappa, and B. S. J. Prakash, Catal. Commun. **8**, 241 (2007).